communications earth & environment

Article

https://doi.org/10.1038/s43247-024-01957-9

Field evidence of flocculated sediments on a coastal algal reef

Check for updates

Zhi-Cheng Huang [1,2] ✉, Tian-Jian Hsu [3] & Trung Nguyen Ly [1,4]

Flocculation of sediments is crucial for morphodynamics, biogeochemical cycles, and ecological processes in aquatic environments. Here we present field evidence that bio-cohesion primarily drives the flocculation of suspended sediments on a coastal algal reef. Results from concurrent measurements of sediment mass and volume concentrations, along with Reynolds stress, reveal unexpected trends, and the data deviate from the classic Rouse formula when non-cohesive sediment is assumed. Direct estimates of particle effective density show a dependence on mean particle diameter, with a fractal dimension of 2.18. The reduced effective density (or settling velocity) and low fractal dimension are typical of flocs containing lower-density saltwater and organic materials. Additionally, organic content negatively correlates with effective density and positively correlates with the mean particle diameter, confirming that bio-cohesion drives the observed flocculation. These results provide quantitative evidence that organic matter promotes macrofloc formation and floc size growth in a reef environment.

In modern reef ecosystems, crustose coralline algae contribute importantly alongside corals as primary reef builders. Variations in environmental conditions within coral reef ecosystems can result in CCA-dominated habitats or entire regions built by CCA, known as algal reefs[1]. Similar to coral reefs, algal reefs provide a coastal habitat for a diverse range of marine organisms[1–5]. Both CCA and corals are known to be highly sensitive to sediments[6,7]. Reef ecosystems can be damaged by elevated suspended sediment concentration (SSC), or termed suspended particulate matter, i.e., irregular natural aggregates composed of organic matter (OM) and mineral sediments[8–10], due to bleaching that reduces growth rates of corals and alters biological, biochemical, and physical functions of marine organisms[6,11]. Therefore, understanding the mechanisms that govern local sediment dynamics is crucial for preserving these ecosystems and reacting to changes in biological activity caused by climate change.

There is a rich literature on coral reef sediments focusing on examining the correlation between SSC, sediment trapping rates, and local waves and currents[12–15]. However, few studies have simultaneously quantified sediment properties and hydrodynamic drivers, leaving critical knowledge gaps in sediment suspension, settling, and transport mechanisms[16,17]. For instance, flocculation controls the settling velocity of suspended sediment and dictates the health of an ecosystem via sedimentation. While some studies have argued that flocculation may occur in coral reefs[18,19], most studies on sediment dynamics in coral reefs typically assume sediments to be non-cohesive[20–22]. Hence, the physical evidence, transport properties, and formation mechanisms of flocculated sediment in reef systems remain lacking.

Floc dynamics have been widely studied in aquatic environments such as rivers and estuaries[23]. For instance, variations in SSC and particle size distribution (PSD) are studied to highlight the importance of flocs in sediment fluxes and composition[24–26]. The gradient of floc concentration can be related to hydrodynamic stresses and settling velocity using Rouse's formula[27–31]. However, the impact of OM on floc dynamics remains only partially understood[32,33]. Evidence from laboratory studies[33–35] and field observations in estuaries and nearshore waters[36–38] indicates that bio-cohesion affects floc size distribution, enhances stickiness, promotes flocculation of suspended sediment, and alters floc PSD.

While recent studies have emphasized the role of bio-cohesion in promoting floc formation in estuaries, rivers, and sandy/muddy coasts[30,37,39], there is still limited study of floc dynamics in reefs, which are organic-rich coastal environments. In the observations presented below, we report the quantified characteristics of flocs from a coastal algal reef. Vertical profiles of SSC are examined using the Rouse formula. By analyzing microscope images, PSDs measured at two vertical positions, and organic content (OC), we concluded that bio-cohesion plays a crucial role in determining floc properties and the resulting settling velocities.

[1]Graduate Institute of Hydrological and Oceanic Sciences, National Central University, Taoyuan, Taiwan. [2]Graduate Institute of Environmental Engineering, National Central University, Taoyuan, Taiwan. [3]Civil, Construction and Environmental Engineering, Center for Applied Coastal Research, University of Delaware, Newark, DE, USA. [4]College of Environment and Natural Resources, Can Tho University, Can Tho, Vietnam. ✉e-mail: zchuang@ncu.edu.tw

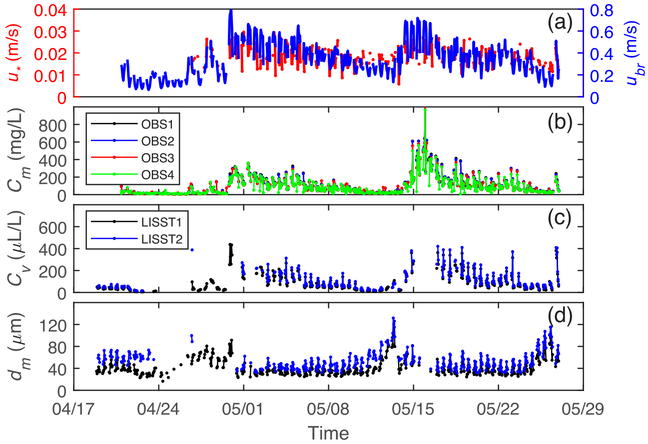

Fig. 1 | Time-series of hydrodynamic and suspended sediment conditions. **a** Friction velocities estimated by the eddy covariance method at ADV2 (0.3 m above the bottom) and root-mean-square wave orbital velocity estimated by the linear wave theory. **b** Mass concentration, C_m measured by OBS1 to OBS4 located at 0.15 m, 0.3 m, 0.52 m, and 0.77 m above the bottom, respectively; **c** bulk volume concentration, C_v, and **d** mean diameter, d_m of suspended sediment measured by LISST1 and LISST2 located at 0.2 m and 0.4 m above the bottom.

Results

Hydrodynamics and suspended sediments

The study was conducted in the intertidal zone of an algal reef located in Taoyuan, northern Taiwan (25° 2'40.44" N, 121° 3'25.21" E). The reef is mainly created by CCA, providing habitat for a diverse algal-reef ecosystem, which has been declared a marine protection area along the coast[2,3,5,40]. The main field experiment (Supplementary Fig. S1) was conducted from April 20th to May 27th, 2022 (38 days). To supplement the data and strengthen the findings, we designed another one-tidal-cycle field experiment (Exp2) to measure OC on January 7, 2023.

Turbulent mixing in most coastal reefs is driven by both mean currents and surface waves[41]. At the study site, surface waves, along with tidal currents, play an important role in generating boundary-layer turbulence and driving sediment suspension quantified by friction velocity (see hydrodynamic data in Methods). The friction velocity estimated using the eddy covariance method u_{*R} agrees with that obtained by the log profile fit u_{*L} (see Supplementary Fig. S2). Figure 1a shows the time series of u_{*R} and root-mean-square wave orbital velocity. While the semidiurnal fluctuation can be identified due to tidal current, the overall magnitude modulation u_{*R} is correlated with the wave orbital velocity.

From the time series of sediment mass concentration C_m at four different elevations measured by OBSs (Fig. 1b), we observe the expected negative vertical gradients away from the bottom. On the contrary, from the time series of particle bulk volume concentration, C_v, the value recorded by LISST2 located at 0.4 m above the bottom (blue dots in Fig. 1c) is almost always larger than that of LISST1 (black dots) located at 0.2 m above the bed, suggesting a positive concentration gradient. Remarkably, there is a difference in measured mean particle size d_m from the two LISST sensors; the particle size d_m is larger for LISST2 located higher in the water column. The surprising observation of larger particle volume concentration and particle sizes higher in the water column while the mass concentration remains lower may be explained by the possibility that sediments are flocculated. As the higher-density mineral particles form flocs with their sizes much larger than the individual mineral particles, the volumetric concentration of particles (flocs) seen by LISST increases and it is consistent with the increased particle size observed. Meanwhile, the increased pore space in the flocs may be filled with pore water and organic materials of lower densities. We hypothesize that suspended particles may contain low-density components due to flocculation and the following results will prove this point and strengthen the evidence that observed sediments in the algal reef are flocculated.

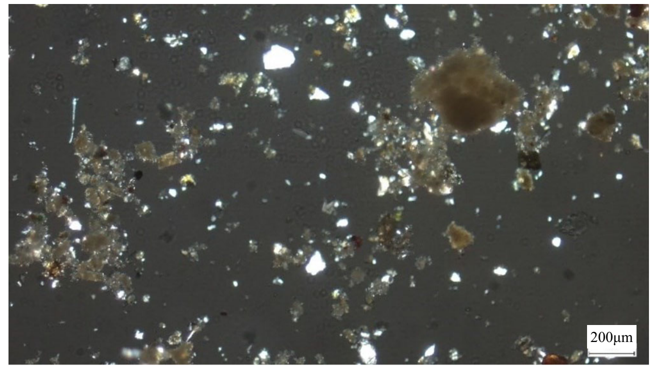

Fig. 2 | A sample of a microscopic view of the collected suspended sediment. The brightly colored objects in the photos represent mineral particles, while the darker colors represent OM.

Evidence from microscope images

A micro-CT scanner is useful for performing three-dimensional reconstructions of flocs to understand their internal porosity and compositional structures[8,42–44]. For qualitative but direct evidence, we used a microscope to examine the suspended particles in the collected water samples as illustrated in Fig. 2, where the bright-colored objects represent mineral particles, while the dark-colored materials represent OM. The photos show that, in addition to crystalline quartz, there is an abundance of irregular, gelatinous-like substances, which are recognized as OM, or biofilms (extracellular polymeric substances). These OMs sometimes bond with silica-like particles to form larger aggregates. Typical specific weights of OMs are much smaller than mineral particles, almost close to water. For example, tests conducted in biological reactors found that the wet density of biofilm is about 1000–1140 kg m^{-3} (ref. 45). The density of OM is assumed to be 1000 kg m^{-3} in estuarine surface water[36]. How does the OM connect mineral particles and generate flocs with reduced effective density?

Evidence from floc effective density

Particle settling velocity can be estimated from the mass concentration data measured at different vertical elevations by comparing with the theoretical Rouse concentration profile[27,29]:

$$\frac{c_m}{C_{m,a}} = \left[\frac{a(h-z)}{z(h-a)}\right]^{\beta}, \tag{1}$$

where $C_{m,a}$ is a reference mass concentration of sediment at a height $z = a$ above the bed, h is the water depth, and β is the Rouse number defined as:

$$\beta = \frac{w_s}{\kappa u_*}. \tag{2}$$

where w_s is the particle settling velocity, $\kappa = 0.41$ is the Karman constant, and u_* is the friction velocity estimate hereby u_{*R} or u_{*L} using two different methods discussed in Supplementary Fig. S2. By adjusting β the Rouse profile to fit with the measured sediment mass concentration profile (with a quality control of R^2 value greater than 0.85), we obtain β_{obs} from the observed data that the corresponding particle settling velocity can be back-calculated via Eq. (2).

In studies of non-cohesive sediment transport, the settling velocity can be estimated by a widely used empirical formula as follows[22,46]:

$$w_s = \frac{\nu}{d_m}\left(\sqrt{10.36D_*^2 + 1.049D_*^3} - 10.36\right), \tag{3}$$

where D_* is the dimensionless grain size, $D_* = [(\rho_s - \rho_w)/\rho_w \cdot (g/\nu^2)]^{1/3} d_m$, g is the gravitational acceleration, ν is

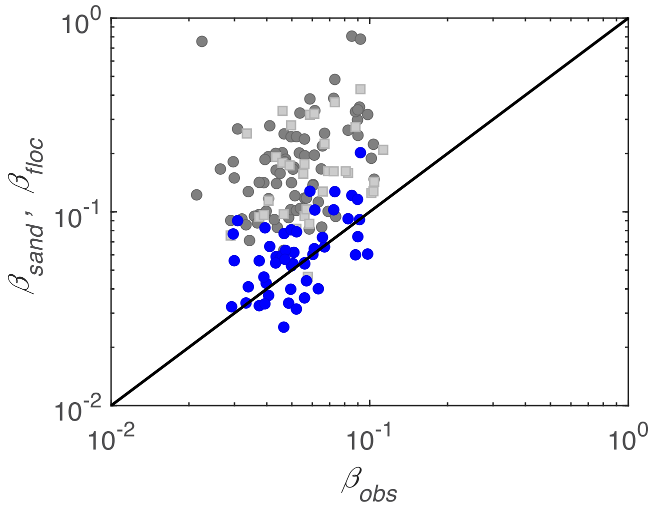

Fig. 3 | Scatterplot of Rouse number (β_{obs}) estimated from Rouse profile-fits of SSC vs Rouse number (β_{sand} and β_{floc}) estimated by friction velocity (u_*) and settling velocity (w_s). β_{sand} is estimated by $w_s/(\kappa u_*)$ with w_s determined by classic formula with non-cohesive sediment density, where dark gray circles and light gray squares are u_* estimated by methods of eddy covariance (u_{*R}) and log-profile-fits (u_{*L}), respectively. The blue circles are β_{floc} calculated using u_{*R} and w_s with effective density estimated by LISST and OBSs (cohesive sediment, to be discussed latter).

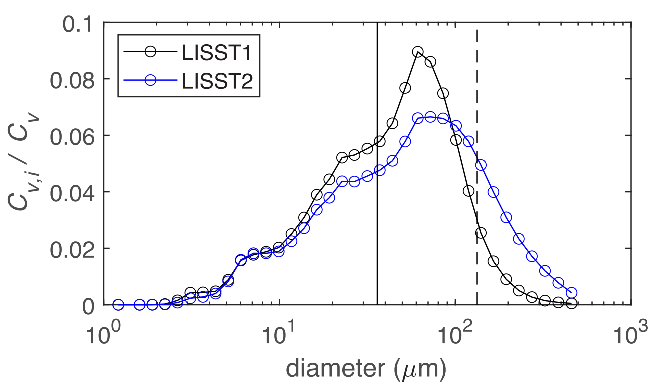

Fig. 4 | Averaged particle size distribution measured by the two LISSTs. The distribution is quantified by the particle volumetric concentration in each size class bin normalized by the bulk volumetric concentration. The vertical black solid and dashed lines signify the diameters of 36 μm and 133 μm.

the kinematic viscosity of seawater (m^2 s^{-1}), ρ_w= 1030 kg m^{-3} is seawater density, and the density for non-cohesive sediment is specified to be ρ_s = 2650 kg m^{-3}. Using the non-cohesive sediment settling calculated via Eq. (3) and measured friction velocity (u_{*R} or u_{*L}), the resulting Rouse number β_{sand} does not agree with the obtained β_{obs} from the measured data (Fig. 3). In fact, β_{sand} is larger than β_{obs} with a factor ranging from 1.34 to 17.34 and a mean value of β_{sand}/β_{obs} = 3.93 ± 2.22 (R^2 = 0.27), suggesting that the estimated settling velocity using Eq. (3) for noncohesive sediment is much larger than the measured value and most likely due to using a non-cohesive sediment density of ρ_s= 2650 kg m^{-3}. Results reported here are similar to those presented by Lamb et al.[27] who used a similar method to argue that the sediment measured in fluvial environments is flocculated. Using u_{*R} and w_s estimated with an effective density directly calculated from LISST and OBSs, the resulting β_{floc} agrees better with β_{obs} (β_{floc}/β_{obs}= 1.24 ± 0.46, R^2 = 0.29). The reminder of this paper will explain how the effective density is calculated from the measured data and the reason causing the reduced effective density due to flocculation

Unlike non-cohesive sand particles, the density and size distribution of the flocculated aggregates (flocs) are highly variable in the water column. It has been reported that there are four-level groups of flocculated aggerates in coastal water, including primary particles, flocculi, microflocs, and macroflocs. The transitions from flocculi to microflocs and from microflocs to macroflocs are typically defined at 36 μm and 133 μm, respectively[47,48]. From the PSD quantified by the normalized volumetric concentration in each size class bin (Fig. 4), it is clear that there were more flocculi and smaller microflocs (particle diameter < 90 μm) in the lower water column as measured by LISST1 (20 cm above the bed). Remarkably, LISST2 located at 40 cm above the bed measured more macroflocs and larger microflocs (particle diameter > 90 μm) than those at LISST1. The existence of larger-sized particles higher in the water column suggests that the densities of those larger particles are much smaller and reflect the consequence of the flocculation of suspended sediment over the reef. Moreover, higher turbulence in the bottom boundary layer, closer to the bed, encourages floc breakup[49,50] and this qualitatively explains why more macroflocs may exist higher in the water column.

The effective density of flocs, ρ_e, is defined as follows[51,52]:

$$\rho_e = \rho_f - \rho_w = \left(\frac{\rho_s - \rho_w}{\rho_s}\right)\rho_a, \quad (4)$$

where $\rho_f = m_f/V_f$ is the density of flocs, $\rho_a = 10^3 \cdot C_m/C_v$ is the apparent density of flocs. In this study, the mass concentration C_m (mg L^{-1}) is measured by the OBS sensors, and the bulk volume concentration C_v (μL L^{-1}) is measured by the LISST. Namely, the effective density of flocs can be obtained using Eq. (4). The settling velocity of flocs, w_s, is then calculated by Stokes' law[52–54]:

$$w_s = \frac{\rho_e g}{18\,\mu} d_m^2, \quad (5)$$

where μ= 10^{-3} kg m^{-1} s^{-1} is the dynamic viscosity of seawater.

Figure 5 shows the computed ρ_e and w_s as a function of d_m. The observed ρ_e varied between 100 kg m^{-3} and 1050 kg m^{-3} in the size range of 25–100 μm (Fig. 5a), which are smaller than that of sand in seawater (1620 kg m^{-3}, dashed line in Fig. 5a). Statistically significant negative correlations between ρ_e and d_m with r of −0.80 (p < 0.001) are found in the measured data. This negative correlation signifies the increase of pore space in the floc, filled with lower-density pore water and OM, as the floc size increases. The results w_s computed using Stokes' law (Eq. (5)) are in the range from 0.2 mm s^{-1} to 2 mm s^{-1}, which is also smaller than that of sand (dashed line in Fig. 5b). A high correlation between w_s and d_m is obtained with r of 0.89 (p < 0.001) are found for data of LISST1 and 2.

Incorporating self-similar fractal theory with the three-dimensional fractal dimension denoted as F, the effective density of floc ρ_e scales with $\sim d_m^{F-3}$ (ref. 54) and hence the scaling relationship for floc settling velocity is $w_s \sim d_m^{F-3}$ (refs. 55,56). From the measured ρ_e or w_s shown in Fig. 5, we can further estimate F by calculating the slope of the regression lines. For the regression of all data, we obtain F= 2.18 (R^2 = 0.64 and 0.79 for ρ_e and w_s). Data grouped by size between 60 μm and 70 μm, F ranges from 2.26 to 2.28 (dark gray line) for the smaller size group and from 1.75 to 1.81 (light gray line) for the larger size group with R^2 = 0.66 and 0.80. Typical F values for flocs fall within the range of 1.8–2.2 (ref. 36).

The settling velocity calculated by using the Rouse number β_{obs} estimated from the Rouse-profile-fit of measured SSC via Eq. (2) (see Fig. 3) also agrees with the settling velocity calculated ρ_e directly estimated from the measured data (gray line in Fig. 5b). The computed floc effective density and settling velocity, as well as the resulting fractal dimension indicates strong evidence of flocculation over the coastal reef.

Discussion and conclusions

We have presented compelling evidence that suspended sediments on the algal reef off the coast of Taoyuan in northern Taiwan are flocculated. While many studies have investigated flocculation in rivers and estuaries[24,25,27–31,36–39], the data presented in this study revealed and quantified the flocculation characteristics of suspended sediment in reef environments.

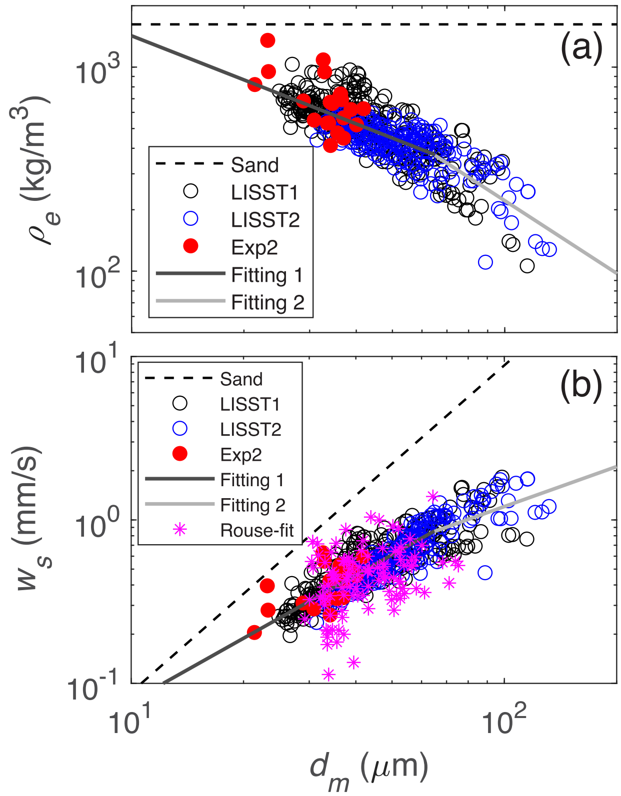

Fig. 5 | Floc characteristics as a function of mean particle (floc) diameter, d_m. **a** Effective density, ρ_e, and **b** settling velocity, w_s. The gray lines are fitting curves for the data of LISST1 and 2; the dashed black line in (**a**, **b**) is the ρ_e and w_s of sand. The purple stars are the w_s estimated from Eq. (2) using β calculated by fitting the measured data with the Rouse profile.

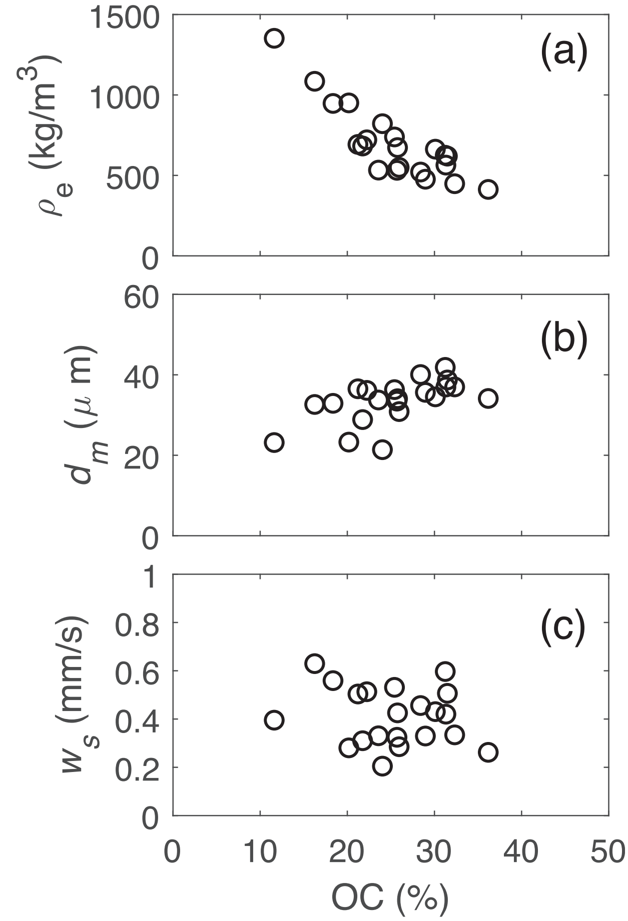

Fig. 6 | Floc characteristics as a function of organic content, OC. **a** Effective density, ρ_e, **b** mean diameter, d_m, and **c** settling velocity, w_s. The data is obtained in the Exp. 2.

The observed effective densities and settling velocities of flocs are much smaller than those of non-cohesive sediments, and strongly correlate with mean diameters of flocs with a fractal dimension clearly decreasing for larger microflocs and macroflocs.

Flocs observed in the field are of high porosity, three-dimensional structures that contain low-density OM and seawater[8,43]. While the evidence of flocculation is established at this particular algal reef site, it is important to address the main cause of flocculation so that the findings can be generalized. Floc formations are typically due to the presence of functional groups from clay minerals in saltwater and transparent exopolymer particles (or more generally the extracellular polymeric substance)[57]. We used X-ray diffraction analysis to analyze the sediment samples and found that the proportion of clay minerals was relatively small (about 3%, Supplementary Fig. S3). From the data using the weight loss on ignition method in the Exp2, the weight proportion of the OM to total suspended matter was found to be about 12–36% in the study site. This is consistent with the microscope image (see Fig. 2) showing that OMs would form a sticky substance with transparent exopolymer particles[58,59] and connect mineral particles. Figure 6a shows that the effective density negatively correlates with the OC with a high significance ($r = -0.86$, $p < 0.001$); moreover, the mean floc diameter positively correlates with the OC ($r = 0.60$, $p = 0.004$, Fig. 6b). The results suggest that when the OC increases, the stickiness increases and encourages flocculation[60], leading to a greater reduction in the effective density (Fig. 6a). The increase in OC and stickiness also results in a weaker increase in the mean diameter of suspended sediment, consistent with the data reported by Ye et al.[61] that an increase in the OC can reduce the effective density, whereas the increase in particle size is less pronounced. Due to the competing effect between effective density and floc diameter, the dependence of settling velocity on mean floc diameter is weak (Fig. 6c) as we obtain a low correlation ($r = -0.18$, $p = 0.42$). With the dominance of OM, the settling velocity is around 0.2–0.6 mm s^{-1}.

The simultaneously measured PSDs at two different vertical locations show higher volume concentrations in the size range of macroflocs in the upper water column, while the overall mass concentration is lower. This directly infers a reduction of mineral constituents in macroflocs, or in other words, a much lower effective density compared to the microfloc counterpart. The observed PSDs show a non-unimodal peak distribution, resembling the result of interactions among multiple modal peaks[24,25,37,39,48,61]. This pattern is not characteristic of the fractal behavior typically seen in uniform mineral flocs. The flocculation observed here is primarily promoted within the size range of larger microflocs and macroflocs, with OM playing a crucial role in the growth of flocs (Figs. 4 and 6). The aggregation of macroflocs likely involves using flocs in the microfloc size range as fundamental constituent particles[39]. This can be explained by the polymer bridging mechanism formed by an extracellular polymeric substance in the OM[8,61]. These constituent materials of OM include various biologically produced components, leading to complex bio-physical interactions[32] and exhibiting size-independent behavior[8]. In environments influenced by OM, the growth of macroflocs is primarily determined by the nutrient-dependent growth rate and carrying capacity, which is dictated by primary production as a seasonal function of nutrients, light, temperature, and other factors, and influenced by OM, turbulence, and the maximum size of microflocs, respectively[10,39,62]. Moreover, the observed effective density decreases as the flocs grow, with a fractal dimension which is clearly smaller for larger flocs (Fig. 5). These results suggest that flocs grow in a pseudo-fractal manner, dependent on constituent materials produced by OM. This complexity causes the observed flocculation process on the reef to deviate from the predictions of fractal theory for uniform mineral flocs[61].

Laboratory studies[32–34,62,63] and field observations in estuaries and nearshore waters[36–39] have shown that bio-cohesion greatly enhances the stickiness that promotes macrofloc formation and alters the PSD, effective density, and settling velocity. Our findings provide field evidence that OM plays a crucial role in the physical flocculation process and the growth of flocculated sediments. These results support that applying classical fractal theory may be insufficient to fully capture the complexity of the flocculation mechanism[8,61]. The results provide unique and rare field evidence on the occurrence of cohesive sediment flocculation on a coastal reef due to the dominance of bio-cohesion. Since flocculation with bio-cohesion changes how the settling velocity is estimated, more extensive future research is anticipated to improve the predictions of sediment transport in organic-rich reef environments.

In the algal reef environment, algae[64], SSC, and hydrodynamics[14] all exhibit seasonal variations. In addition to biological factors that depend on the season, changes in turbulence production in reef environments, caused by mechanisms such as wave-breaking and colony-scale enhanced wakes, may alter boundary-layer-generated turbulence. This, in turn, could affect the adhesion mechanisms between microflocs and macroflocs in our study. Similar to other field studies showing seasonal variations in floc dynamics[29,65], future studies are needed to explore potential seasonal variations in OC and floc characteristics on the reef.

Methods

Instrumentation and setup

The main experiment and the supplemental experiment are a result of a real-time and long-term monitoring project initiated in 2019[14]. Four 6M-Hz acoustic Doppler velocimetries (ADV, Nortek Vector) were mounted in a vertical array to measure the tides, waves, currents, and turbulence as shown in Supplementary Fig. S1. Two ADCPs (Nortek Signature 1000) were installed up-looking and down-looking on the reef seabed near the ADV array, respectively.

The sediment mass concentration, C_m (mg L^{-1}), was measured using four optical backscatter sensors (OBS, Campbell Scientific, OBS-3+, and ClariVUE10) that were oriented sideways with ADVs. Two LISST-200x submersible laser diffraction particle size analyzers (Sequoia Scientific), as shown in Supplementary Fig. S1, measured 36 size classes of particle volume concentration denotes $C_{v,i}$ (μL L^{-1}) and their summation is the bulk volume concentration, C_v (μL L^{-1}). A more detailed discussion of the instruments, data processing methods, and results is provided in Supplementary Fig. S4.

A total of 21 data samples were collected in the supplemental experiment (Exp2). Some of the water samples were immediately observed and photographed on-site using a microscope, while others were analyzed in the laboratory using the weight loss on ignition method. The marine samples (2.05 L) were diluted with deionized water to remove salt, and heated at 105 °C for 12 h to remove the moisture and obtain the total mass of suspended particulate matter (organic and inorganic content). The samples were then heated at 550 °C for 12 h to obtain the mass of the inorganic content[36,66]. The OC (%) is defined as the ratio of the weight loss using the ignition method from 105 °C to 550 °C, divided by the total weight at 105 °C.

Estimates of friction velocity

Two methods were used to estimate the friction velocities: (1) eddy covariance, and (2) log-profile-fit techniques. The turbulent fluctuations were obtained using differencing technique[67,68]. The eddy covariance technique directly uses the decomposed turbulent fluctuations of ADV data to determine the turbulent Reynolds stresses and friction velocity u_{*R}. The log-profile-fit technique uses six to eleven (between 0.3 m and 2.54 m above the bottom, depending on the tidal elevation) points of time-averaged mean currents, including data from the ADV (ADV2-4) and the two ADCP measurements to fit the log profile and obtain the corresponding friction velocity u_{*L}. To ensure a well-defined logarithmic region over the measurement points used in the fit, only profiles with an R^2 value greater than 0.9 were included in the analysis. More descriptions and results of the Log-profile-fit technique are provided in Supplementary Fig. S2.

Hydrodynamic data

Supplementary Fig. S5 presents an overview of the measured time series of several important quantities during the experiment period. The variation in the local water depth, h, is mainly caused by the semidiurnal tide (Supplementary Fig. S5a). Note that data with a water depth of less than 0.9 m were excluded because the highest instrument was positioned at 0.7 m. The significant wave heights, H_s, computed using pressure data, vary from 0 m to 1.5 m (Fig. 2b). Considering the wave breaking index H_s/h = 0.42, results indicate that the observed data are mostly under non-breaking waves. Only a few data during high waves on May 1st and 16th may be affected by weakly spilling breaking waves. Measured time series of the depth-averaged mean current intensity, U_c is highly correlated with water level driven by the semidiurnal tide (compare Supplementary Fig. S5a, c). This is consistent with Delft-3D numerical modeling to study the effects of wind, waves, and tides on driving the coastal currents[68], which shows that the measured coastal currents are mostly due to tides because of the strong tidal currents in the Taiwan Strait. The currents are toward the west direction during flooding tides and then switch toward the east–south–east direction during ebbing tides at the study site. The wave-induced velocities (Fig. 1a) were estimated by the representative root-mean-square near-bottom velocity, u_{br}, using linear-wave theory for spectral waves[69,70]. The ratio between u_{br} and U_c ranges from 0 to 22 with a mean of 2.9 and std of 2.55 and the wave-induced motions are greater than the mean current velocity due to the energetic shallow water condition.

Data availability

The data are available at: https://doi.org/10.6084/m9.figshare.27289275.

Received: 23 July 2024; Accepted: 6 December 2024;
Published online: 07 January 2025

References

1. Cornwall, C. E. et al. Crustose coralline algae can contribute more than corals to coral reef carbonate production. *Commun. Earth Environ.* **4**, 105 (2023).
2. Yu, H. Y., Huang, S. C. & Lin, H. J. Factors structuring the macrobenthos community in tidal algal reefs. *Mar. Environ. Res.* **161**, 105119 (2020).
3. Kuo, C. Y. et al. Demographic census confirms a stable population of the critically-endangered caryophyllid coral *Polycyathus chaishanensis* (Scleractinia; Caryophyllidae) in the Datan Algal Reef, Taiwan. *Sci. Rep.* **10**, 10585 (2020).
4. Nazir, A. et al. Anthropogenic nitrogen pollution inferred by stable isotope records of crustose coralline algae. *Mar. Pollut. Bull.* **198**, 115839 (2024).
5. Liou, C. Y., Yang, S. Y. & Chen, C. A. Unprecedented calcareous algal reefs in northern Taiwan merit high conservation priority. *Coral Reefs* **36**, 1253–1253 (2017).
6. Bainbridge, Z. et al. Fine sediment and particulate organic matter: a review and case study on ridge-to-reef transport, transformations, fates, and impacts on marine ecosystems. *Mar. Pollut. Bull.* **135**, 1205–1220 (2018).
7. Fabricius, K. & De'ath, G. Environmental factors associated with the spatial distribution of crustose coralline algae on the Great Barrier Reef. *Coral Reefs* **19**, 303–309 (2001).
8. Spencer, K. L. et al. A structure-function based approach to floc hierarchy and evidence for the non-fractal nature of natural sediment flocs. *Sci. Rep.* **11**, 14012 (2021).
9. Burd, A. B. & Jackson, G. A. Particle aggregation. *Annu. Rev. Mar. Sci.* **1**, 65–90 (2009).
10. Maggi, F. Biological flocculation of suspended particles in nutrient-rich aqueous ecosystems. *J. Hydrol.* **376**, 116–125 (2009).

11. Rogers, C. S. Responses of coral reefs and reef organisms to sedimentation. *Mar. Ecol. Prog. Ser.* **62**, 185–202 (1990).
12. Ogston, A. S., Storlazzi, C. D., Field, M. E. & Presto, M. K. Sediment resuspension and transport patterns on a fringing reef flat, Molokai, Hawaii. *Coral Reefs* **23**, 559–569 (2004).
13. Storlazzi, C. D., Field, M. E., Bothner, M. H., Presto, M. K. & Draut, A. E. Sedimentation processes in a coral reef embayment: Hanalei Bay, Kauai. *Mar. Geol.* **264**, 140–151 (2009).
14. Ly, T. N. & Huang, Z. C. Real-time and long-term monitoring of waves and suspended sediment concentrations over an intertidal algal reef. *Environ. Monit. Assess.* **194**, 839 (2022).
15. Larcombe, P., Ridd, P. V., Prytz, A. & Wilson, B. Factors controlling suspended sediment on inner-shelf coral-reefs, Townsville, Australia. *Coral Reefs* **14**, 163–171 (1995).
16. Schlaefer, J. A., Tebbett, S. B. & Bellwood, D. R. The study of sediments on coral reefs: a hydrodynamic perspective. *Mar. Pollut. Bull.* **169**, 112580 (2021).
17. Tebbett, S. B. et al. Bio-physical determinants of sediment accumulation on an offshore coral reef: a snapshot study. *Sci. Total Environ.* **895**, 165188 (2023).
18. Livsey, D. L., Crosswell, J. R., Turner, R. D. R., Steven, A. D. L. & Grace, P. R. Flocculation of riverine sediment draining to the great barrier reef, implications for monitoring and modeling of sediment dispersal across continental shelves. *J. Geophys. Res. Oceans* **127**, e2021JC017988 (2022).
19. Jouon, A. et al. Spatio-temporal variability in suspended particulate matter concentration and the role of aggregation on size distribution in a coral reef lagoon. *Mar. Geol.* **256**, 36–48 (2008).
20. Rosenberger, K. J. et al. Spectral wave-driven bedload transport across a coral reef flat/lagoon complex. *Front. Mar. Sci.* **7**, 513020 (2020).
21. Pomeroy, A. W. M. et al. The contribution of currents, sea-swell waves, and infragravity waves to suspended-sediment transport across a coral reef-lagoon system. *J. Geophys. Res. Oceans* **126**, e2020JC017010 (2021).
22. Pomeroy, A. W. M. et al. Sediment transport in the presence of large reef bottom roughness. *J. Geophys. Res. Oceans* **122**, 1347–1368 (2017).
23. Manning, A. J., Langston, W. J. & Jonas, P. J. C. A review of sediment dynamics in the Severn estuary: influence of flocculation. *Mar. Pollut. Bull.* **61**, 37–51 (2010).
24. Piton, V. et al. From particles to flocs: revealing where flocculation occurs in the nearfield of a negatively-buoyant river plume in a large lake (Lake Geneva). *J. Geophys. Res. Oceans* **129**, e2023JC019860 (2024).
25. Allen, R. M., Livsey, D. N. & McGill, S. C. Observations of flocs in an estuary and implications for computation of settling velocity. *J. Geophys. Res. Oceans* **129**, e2022JC019402 (2024).
26. Pearson, S. G. et al. Characterizing the composition of sand and mud suspensions in coastal and estuarine environments using combined optical and acoustic measurements. *J. Geophys. Res. Oceans* **126**, e2021JC017354 (2021).
27. Lamb, M. P. et al. Mud in rivers transported as flocculated and suspended bed material. *Nat. Geosci.* **13**, 566–570 (2020).
28. Egan, G., Chang, G., Manning, A. J., Monismith, S. & Fringer, O. On the variability of floc characteristics in a shallow estuary. *J. Geophys. Res. Oceans* **127**, e2021JC018343 (2022).
29. Osborn, R., Dunne, K. B. J., Ashley, T., Nittrouer, J. A. & Strom, K. The flocculation state of mud in the lowermost freshwater reaches of the mississippi river: spatial distribution of sizes, seasonal changes, and their impact on vertical concentration profiles. *J. Geophys. Res. Earth Surf.* **128**, e2022JF006975 (2023).
30. Dunne, K. B. J., Nittrouer, J. A., Abolfazli, E., Osborn, R. & Strom, K. B. Hydrodynamically-driven deposition of mud in river systems. *Geophys. Res. Lett.* **51**, e2023GL107174 (2024).
31. Nghiem, J. A., Fischer, W. W., Li, G. K. & Lamb, M. P. A Mechanistic model for mud flocculation in freshwater rivers. *J. Geophys. Res. Earth Surf.* **127**, e2021JF006392 (2022).
32. Guo, C. et al. On the role of organic matter composition in fresh-water kaolinite flocculation. *J. Environ. Manag.* **345**, 118576 (2023).
33. Ye, L., Penaloza-Giraldo, J. A., Manning, A. J., Holyoke, J. & Hsu, T. J. Biophysical flocculation reduces variability of cohesive sediment settling velocity. *Commun. Earth Environ.* **4**, 138 (2023).
34. Zhu, Y. L. et al. Biomineral flocculation of kaolinite and microalgae: laboratory experiments and stochastic modeling. *J. Geophys. Res. Oceans* **127**, e2022JC018591 (2022).
35. Abolfazli, E. & Strom, K. Salinity impacts on floc size and growth rate with and without natural organic matter. *J. Geophys. Res. Oceans* **128**, e2022JC019255 (2023).
36. Fall, K. A., Friedrichs, C. T., Massey, G. M., Bowers, D. G. & Smith, S. J. The importance of organic content to fractal floc properties in estuarine surface waters: insights from video, LISST, and pump sampling. *J. Geophys. Res. Oceans* **126**, e2020JC016787 (2021).
37. Ye, L. P., Huang, M., Liu, H., Gu, J. J. & Wu, J. X. Flocculation under combined effects of hydrodynamic and subaqueous biomass in the bottom boundary layer (BBL) of a microtidal estuary. *Sci. Total Environ.* **913**, 169660 (2024).
38. Fettweis, M. et al. Organic matter composition of biomineral flocs and its influence on suspended particulate matter dynamics along a nearshore to offshore transect. *J. Geophys. Res. Biogeosci.* **127**, e2021JG006332 (2022).
39. Shen, X. T., Toorman, E. A., Lee, B. J. & Fettweis, M. Biophysical flocculation of suspended particulate matters in Belgian coastal zones. *J. Hydrol.* **567**, 238–252 (2018).
40. Liu, L. C., Lin, S. M., Caragnano, A. & Payri, C. Species diversity and molecular phylogeny of non-geniculate coralline algae (Corallinophycidae, Rhodophyta) from Taoyuan algal reefs in northern Taiwan, including Crustaphytum gen. nov. and three new species. *J. Appl. Phycol.* **30**, 3455–3469 (2018).
41. Davis K. A., Pawlak G., Monismith S. G. Turbulence and coral reefs, Vol. 13. In: *Annual Review of Marine Science* (eds. Carlson, C.A. & Giovannoni, S.J.) 343–373 (2001).
42. Lawrence, T. J. et al. Functional behaviour of flocs explained by observed 3D structure and porosity. *Front. Earth Sci.* **11**, 1264953 (2023).
43. Spencer, K. L. et al. Quantification of 3-dimensional structure and properties of flocculated natural suspended sediment. *Water Res.* **222**, 118835 (2022).
44. Lawrence, T. J. et al. A novel 3D volumetric method for directly quantifying porosity and pore space morphology in flocculated suspended sediments. *MethodsX* **10**, 101975 (2023).
45. Ro, K. S. & Neethling, J. B. Biofilm density for biological fluidized beds. *Res. J. Water Pollut. Control Fed.* **63**, 815–818 (1991).
46. Soulsby, R. L. *Dynamics of Marine Sands: A Manual for Practical Applications* (Thomas Telford, London, 1997).
47. Mikkelsen, O. A., Hill, P. S. & Milligan, T. G. Single-grain, microfloc and macrofloc volume variations observed with a LISST-100 and a digital floc camera. *J. Sea Res.* **55**, 87–102 (2006).
48. Lee, B. J., Fettweis, M., Toorman, E. & Molz, F. J. Multimodality of a particle size distribution of cohesive suspended particulate matters in a coastal zone. *J. Geophys. Res. Oceans* **117**, C03014 (2012).
49. Winterwerp, J. C. A simple model for turbulence induced flocculation of cohesive sediment. *J. Hydraul. Res.* **36**, 309–326 (1998).
50. Kuprenas, R., Tran, D. & Strom, K. A shear-limited flocculation model for dynamically predicting average floc size. *J. Geophys. Res. Oceans* **123**, 6736–6752 (2018).
51. Hurley, A. J., Hill, P. S., Milligan, T. G. & Law, B. A. Optical methods for estimating apparent density of sediment in suspension. *Methods Oceanogr.* **17**, 153–168 (2016).

52. Mikkelsen, O. A. & Pejrup, M. The use of a LISST-100 laser particle sizer for in-situ estimates of flee size, density and settling velocity. *Geo-Mar. Lett.* **20**, 187–195 (2001).
53. Winterwerp, J. C., Kessel, T. V., Maren, D. S. V., & Prooijen, B. C. V. *Fine Sediment in Open Water*, vol. 55 (World Scientific, 2022).
54. Manning, A. J. & Dyer, K. R. A laboratory examination of floc characteristics with regard to turbulent shearing. *Mar. Geol.* **160**, 147–170 (1999).
55. Khelifa, A. & Hill, P. S. Models for effective density and settling velocity of flocs. *J. Hydraul. Res.* **44**, 390–401 (2006).
56. Kranenburg, C. The fractal structure of cohesive sediment aggregates. *Estuar. Coast Shelf Sci.* **39**, 451–460 (1994).
57. Malpezzi, M. A., Sanford, L. P. & Crump, B. C. Abundance and distribution of transparent exopolymer particles in the estuarine turbidity maximum of Chesapeake Bay. *Mar. Ecol. Prog. Ser.* **486**, 23–35 (2013).
58. Passow, U. & Alldredge, A. L. Aggregation of a diatom bloom in a mesocosm - the role of transparent exopolymer particles (TEP). *Deep Sea Res. Part II Top. Stud. Oceanogr.* **42**, 99–109 (1995).
59. Engel, A. & Schartau, M. Influence of transparent exopolymer particles (TEP) on sinking velocity of Nitzschia closterium aggregates. *Mar. Ecol. Prog. Ser.* **182**, 69–76 (1999).
60. Engel, A. The role of transparent exopolymer particles (TEP) in the increase in apparent particle stickiness (α) during the decline of a diatom bloom. *J. Plankton Res.* **22**, 485–497 (2000).
61. Ye, L. P., Wu, J. X., Huang, M. & Yan, J. The role of suspended extracellular polymeric substance (EPS) on equilibrium flocculation of clay minerals in high salinity water. *Water Res.* **244**, 120451 (2023).
62. Shen, X. T., Toorman, E. A., Lee, B. J. & Fettweis, M. An approach to modeling biofilm growth during the flocculation of suspended cohesive sediments. *J. Geophys. Res. Oceans* **124**, 4098–4116 (2019).
63. Abolfazli, E., Osborn, R., Dunne, K. B. J., Nittrouer, J. A. & Strom, K. Flocculation characteristics of suspended Mississippi river mud under variable turbulence, water and salt sources, and salinity: a laboratory study. *Front. Earth Sci.* **12**, 1268992 (2024).
64. Lin, S.-M., Tseng, L.-C., Ang, P. O., Bolton, J. & Liu, L.-C. Long-term study on seasonal changes in floristic composition and structure of marine macroalgal communities along the coast of Northern Taiwan, southern East China Sea. *Mar. Biol.* **165**, 1–1 (2018).
65. Horemans, D. M. L. et al. Seasonal variations in flocculation and erosion affecting the large-scale suspended sediment distribution in the scheldt estuary: the importance of biotic effects. *J. Geophys. Res. Oceans* **126**, e2020JC016805 (2021).
66. Wang, Q. R., Li, Y. C. & Wang, Y. Optimizing the weight loss-on-ignition methodology to quantify organic and carbonate carbon of sediments from diverse sources. *Environ. Monit. Assess.* **174**, 241–257 (2011).
67. Shaw, W. J. & Trowbridge, J. H. The direct estimation of near-bottom turbulent fluxes in the presence of energetic wave motions. *J. Atmos. Ocean. Technol.* **18**, 1540–1557 (2001).
68. Lan, Y. R. & Huang, Z. C. Numerical modeling on wave–current flows and bed shear stresses over an algal reef. *Environ. Fluid Mech.* **24**, 697–718 (2024).
69. Madsen O. S. Spectral wave-current bottom boundary layer flows. 24th Int. Conf. Coastal Eng.; 1994: ASCE; 1994. p. 623-634.
70. Huang Z. C., et al. Dissipation of wave energy and turbulence in a barrier-reef lagoon. *Journal of Geophysical Research-Oceans*, **117**, C03015 (2012).

Acknowledgements
We thank Professor L.W. Kuo from the Department of Earth Sciences at National Central University for assisting with the X-ray diffraction analysis of the sediments. Z.-C.H. was supported by the National Science and Technology Council in Taiwan under grant number NSTC 112-2621-M-008-004. T.-J.H. is supported by the U.S. National Science Foundation (OCE-1924532). We thank CPC and the Taoyuan City Government for their support in research funding from related projects. The authors would like to thank the anonymous reviewers for their insightful comments, which have greatly improved the paper.

Author contributions
Z.-C.H. supervised the original project, designed and conducted the field experiments, analyzed the data, and prepared the manuscript. T.-J.L. innovated the topic and advised on the knowledge and analysis of flocculation. T.N.L. conducted the field experiments and performed preliminary analysis. Z.-C.H. and T.-J.H. discussed the results and methods, and contributed to the interpretation of the data and the writing of the paper.

Competing interests
The authors declare no competing interests.

Additional information
Supplementary information The online version contains supplementary material available at https://doi.org/10.1038/s43247-024-01957-9.

Correspondence and requests for materials should be addressed to Zhi-Cheng Huang.

Peer review information *Communications Earth & Environment* thanks T.J. Lawrence and the other, anonymous, reviewer(s) for their contribution to the peer review of this work. Primary Handling Editors: Haihan Zhang and Alireza Bahadori. A peer review file is available.